Atmospheric Environment 177 (2018) 93–99

Contents lists available at ScienceDirect

Atmospheric Environment

journal homepage: www.elsevier.com/locate/atmosenv

Formation of aqueous-phase sulfate during the haze period in China: Kinetics and atmospheric implications

Haijie Zhang[a], Shilu Chen[a], Jie Zhong[b], Shaowen Zhang[a], Yunhong Zhang[a], Xiuhui Zhang[a,*], Zesheng Li[a,**], Xiao Cheng Zeng[b]

[a] Key Laboratory of Cluster Science, Ministry of Education of China, School of Chemistry and Chemical Engineering, Beijing Institute of Technology, Beijing 100081, People's Republic of China

[b] Department of Chemistry, University of Nebraska-Lincoln, Lincoln, NE 68588, United States

ARTICLE INFO

Keywords:
Sulfate
Mechanism
Haze problems
Nitrogen chemistry

ABSTRACT

Sulfate is one of the most important components in the aerosol due to its key role in air pollution and global climate change. Recent work has suggested that reactive nitrogen chemistry in aqueous water can explain the missing source of sulfate in the aqueous water. Herein, we have mapped out the energy profile of the oxidization process of SO_2 leading from NO_2 and two feasible three-step mechanisms have been proposed. For the oxidation of $HOSO_2^-$ and HSO_3^- by the dissolved NO_2 in weakly acidic and neutral aerosol (pH ≤ 7), the main contribution to the missing sulfate production comes from the oxidation of $HOSO_2^-$. The whole process is a self-sustaining process. For the oxidation of SO_3^{2-} in alkaline aerosol (pH > 7), the third step - decomposition step of H_2O or hydrolysis of SO_3 step which are two parallel processes are the rate-limiting steps. The present results are of avail to better understand the missing source of sulfate in the aerosol and hence may lead to better science-based solutions for resolving the severe haze problems in China.

1. Introduction

Air pollution has been recognized as major threat to the human health, especially the persistent haze shrouding North China Plain (NCP) during cold winter. The concentration of PM2.5 (particulate matter with a diameter of less than 2.5 μm) could reach beyond 300 $\mu g\,m^{-3}$ during the most polluted periods. Because of their small sizes, aerosol particles can penetrate into human lungs deeply, causing respiratory diseases, decreasing lung function, and increasing risk of cancer and mortality. Low mixing heights, high relative humidity (RH), large primary pollutants emission and fast secondary inorganic aerosols productions are the major features of winter haze events (Cheng et al., 2016; Xue et al., 2016; Ajdari et al., 2016; Huang et al., 2014; Wang et al., 2016; Li et al., 2016, 2017; Liu et al., 2017). The production rate of sulfate expressed as the concentration ratios of sulfate to sulfur dioxide ($[SO_4^{2-}]/[SO_2]$) increases up to six times higher during the most polluted periods than that during clean to moderately polluted periods (Cheng et al., 2016; Zheng et al.,).

A considerable amount of work has been done on the sulfate formation, nevertheless, there are still major gaps between outdoor measurements and air quality models results (Zheng et al., 2015; Zhang et al., 2015; Shen and Rochelle, 1998; Gao et al.,). Traditional air quality models usually comprise oxidation processes of SO_2 by hydroxyl radical (OH) in gas-phase and by peroxides (H_2O_2) and ozone (O_3) in cloud water or fog droplets (Rohrer and Berresheim,; Laskin et al., 2003; Hoyle et al., 2016). During haze events, most oxidant concentrations decrease because of the aerosol dimming effect, resulting in the decrease of photooxidation (Cheng et al., 2016; Wang et al., 2016; Li et al., 2005, 2016; Tie et al., 2003; Lee and Schwartz, 1982; Clifton et al., 1988). Hence a missing source of sulfate has been suggested recently to explain the sulfate production under the reduced photooxidation level where the trapped SO_2 in the aqueous water is oxidized by the dissolved NO_2 under a nearly neutralized aerosol condition (Cheng et al., 2016; Wang et al., 2016; Lee and Schwartz, 1982; Clifton et al., 1988).

However, to our best knowledge, the energy profile of the chemical mechanism for the suggested sulfate production still remains contentious. The lack of such detailed information could hamper our understanding of the missing source of sulfate and finding science-based solutions to resolve the severe haze problems in China. Hence, the

* Corresponding author.
** Corresponding author.
E-mail addresses: 2120131473@bit.edu.cn (H. Zhang), shlchen@bit.edu.cn (S. Chen), jzhong@huskers.unl.edu (J. Zhong), swzhang@bit.edu.cn (S. Zhang), yhz@bit.edu.cn (Y. Zhang), zhangxiuhui@bit.edu.cn (X. Zhang), zeshengli@bit.edu.cn (Z. Li), xzeng1@unl.edu (X.C. Zeng).

https://doi.org/10.1016/j.atmosenv.2018.01.017
Received 19 September 2017; Received in revised form 25 December 2017; Accepted 7 January 2018
Available online 11 January 2018
1352-2310/

detailed reaction mechanism and energy profile of the reactive nitrogen chemistry in aqueous water are investigated in the present study.

Different ionic states of dissolved sulfur (IV) in the solution are thought to display different reaction kinetics (Brown and Barber, 1995; Vchirawongkwin et al., 2012). S (IV) is primarily in the form of $SO_2{\cdot}H_2O$ at very low pH. With the increase of pH, the tautomer bisulfite ($HOSO_2^-$) and sulfonate (HSO_3^-) become the dominate form and at pH > 7, SO_3^{2-} becomes the most important. To take into comprehensive consideration of the aerosol condition that an averaged pH range of 5 ~ 7 was identified during the polluted period in China (Cheng et al., 2016; Xue et al., 2016; Wang et al., 2016; Shi et al., 2017), all three species $HOSO_2^-$, HSO_3^- and SO_3^{2-} are studied in the present work (Cheng et al., 2016; Kahan et al., 2010; Hoffmann, 1986; Spindler et al., 2003). The overall reaction has been proposed to be described by equations (1) and (2), (Cheng et al., 2016; Lee and Schwartz, 1982; Clifton et al., 1988; Spindler et al., 2003).

$$2NO_2(aq) + HSO_3^-(aq) + H_2O(aq) \rightarrow 3H^+(aq) + 2NO_2^-(aq) + SO_4^{2-}(aq) \quad (1)$$

$$2NO_2(aq) + SO_3^{2-}(aq) + H_2O(aq) \rightarrow 2H^+(aq) + 2NO_2^-(aq) + SO_4^{2-}(aq) \quad (2)$$

2. Method

The Gaussian 09 suit of programs was used to perform high-level quantum-chemical calculations (Frisch et al., 2009). In recent years, numerous benchmarks in regard to the performance of different Density Functional Theory (DFT) functionals have proved that M06-2X functional is a reasonable choice for computing thermochemistry and barrier heights of atmospheric relevant systems (Zhao and Truhlar, 2008; Elm et al., 2012; Pereira et al., 2017; Mardirossian and Head-Gordon, 2016). Hence M06-2X/6-311 + +G(3df,3pd) levels of theory were used for all stationary points calculations. Transition states were optimized to ensure the existence of only one single imaginary frequency and intrinsic reaction coordinate (IRC) calculations were also performed to ensure the appropriate pre- and post-reactive complexes (Gonzalez and Schlegel, 1989; Zhang et al., 2014; Sun et al., 2012; Xu et al., 2010). Single point energy was calculated at CCSD(T)-F12/VDZ-F12 level of theory using ORCA program where cc-pVTZ was used for RI approximation (cc-pVTZ/C) and cc-pVDZ-F12 was used for the complete auxiliary basis set part (cc-pVDZ-F12-CABS) (Neese, 2012; Peterson et al., 2008; Yousaf and Peterson, 2008; Lane and Kjaergaard, 2009; Knizia et al., 2009). The conductor-like polarizable continuum model (CPCM) was used both in the configuration optimization and single point calculations to include solvent effect. Note that the real aerosol particle contains numerous different inorganic and organic compounds. What is more, the compositions and the corresponding proportions are difficult to confirm. Hence, the bulk of water solvent with a dielectric constant of 80.4 is used as a structureless polarizable medium (Takano and Houk, 2005; Delabie et al., 2000; Cossi et al., 2003). In the present study, the corrected Gibbs free energies are discussed and calculated as the sum of the binding energy at the CCSD(T)-F12/VDZ-F12 level and the thermal contribution to the Gibbs free energy at the M06-2X/6-311 + +G(3df,3pd) level (Myllys et al., 2017; Elm et al., 2017). Since the computational model is for the case that the reactions occur in the aqueous water, it is reasonable that in the evaluation of the Gibbs free energies, the contribution of translational motion to the entropies was approximated to none (Dong et al., 2017). Details of the electronic energies, Gibbs free energy correction terms at M062X/6-311 + +G(3df,3pd) level of theory, the single point energies, gibbs free energies, the corrected gibbs free energies of the stationary points investigated, the imaginary frequency of transition state structures and Cartesian coordinates of all stationary points investigated are collected in Tables S1–S62 in the Supplementary Information.

3. Result ans discussion

3.1. The potential reaction mechanisms of SO_2 by NO_2 in the aqueous water

Overall, the oxidation processes of $HOSO_2^-$, HSO_3^- and SO_3^{2-} by NO_2 proposed as Eq. (1) and Eq. (2) are three-step reactions which have been identified and shown in Schemes 1–3. Particularly speaking, the first steps of the oxidation of $HOSO_2^-$, HSO_3^- and SO_3^{2-} are totally different where a $H^\bullet$ elimination step (Eq. (3)) has been identified for $HOSO_2^-$ or HSO_3^- and an electron transfer step (Eq. (4)) for SO_2^{3-}. Nevertheless, these two different processes result the same intermediate free radical $SO_3^{\bullet-}$. Two parallelly second steps have been identified and shown in Scheme 2 for intermediate free radical $SO_3^{\bullet-}$ where Eq. (5) is the O-addition step to the generated $SO_3^{\bullet-}$ and Eq. (6) is the electron transfer step from $SO_3^{\bullet-}$ to NO_2. Similarly, two parallelly third steps have been identified and shown in Scheme 3 where Eq. (7) is the decomposition step of H_2O and Eq. (8) is the hydrolysis step of SO_3.

$$HSO_3^- \text{ or } HOSO_2^- (aq) + NO_2 (aq) \rightarrow SO_3^{\bullet-} (aq) + HONO (aq) \quad (3)$$

$$SO_3^{2-} (aq) + NO_2 (aq) \rightarrow SO_3^{\bullet-} (aq) + NO_2^- (aq) \quad (4)$$

Scheme 1. The first step of oxidation of SO_2 by NO_2 in the aqueous water. Eq. (3) is the $H^\bullet$ elimination step from $HOSO_2^-$ or HSO_3^- in weakly acidic and neutral aerosol (pH ≤ 7). Eq. (4) is an electron transfer step from SO_3^{2-} in alkaline aerosol (pH > 7).

$$SO_3^{\bullet-} (aq) + NO_2 (aq) \rightarrow SO_4NO^- (aq) \quad (5)$$

$$SO_3^{\bullet-} (aq) + NO_2 (aq) \rightarrow SO_3 (aq) + NO_2^- (aq) \quad (6)$$

Scheme 2. Two parallelly second steps of the subsequently oxidation of $SO_3^{\bullet-}$ by NO_2 in the aqueous water. Eq. (5) is the O-addition step and Eq. (6) is the electron transfer step.

$$SO_4NO^- (aq) + H_2O (aq) \rightarrow HSO_4^- (aq) + HONO (aq) \quad (7)$$

$$SO_3 (aq) + H_2O (aq) \rightarrow H_2SO_4 (aq) \quad (8)$$

Scheme 3. Two parallelly third steps where Eq. (7) is the decomposition step of H_2O and Eq. (8) is the hydrolysis step of SO_3.

In this case, two parallelly feasible three-steps mechanism (Mechanism I and Mechanism II) have been identified. Mechanism I comprises Eq. (3) ($H^\bullet$ elimination step from $HOSO_2^-$ or HSO_3^- in weakly acidic and neutral aerosol (pH ≤ 7)) or Eq. (4) (an electron transfer step from SO_3^{2-} in alkaline aerosol (pH > 7)) as the first step, Eq. (5) as the second step and Eq. (7) as the third step. Mechanism II shares the same first step (Eq. (3) and Eq. (4)) with Mechanism I and comprises Eq. (6) as the second step and Eq. (8) as the third step. Hence in the following content, the first step of Mechanism I and Mechanism II is analysed in section 3.1.1, the second and third steps of Mechanism I are analysed in section 3.1.2, the second and third steps of Mechanism II are analysed in section 3.1.3.

3.1.1. The first step of mechanism I and mechanism II for the oxidation of SO_2 by NO_2 in aqueous water

The reactant state (React), transition state for the reaction step (TS) and the resulting product (Prod) have been optimized and displayed in Fig. 1 and Fig. 2. Firstly, the $H^\bullet$ elimination step from HSO_3^- or $HOSO_2^-$ (Eq. (3)) in weakly acidic and neutral aerosol (pH ≤ 7) were identified to have two parallel channels with the formation of $Prod_{cis}$ ($SO_3^{\bullet-}$ and *cis*-HONO) and $Prod_{trans}$ ($SO_3^{\bullet-}$ and *trans*-HONO), respectively. As shown in Fig. 1, for the $H^\bullet$ elimination step from HSO_3^-, a lower barrier of 17.6 kcal/mol (TS_{cis} relative to $React_{cis}$) for the formation of *cis*-HONO and a higher barrier of 26.5 kcal/mol (TS_{trans} relative to $React_{trans}$) for the formation of *trans*-HONO have been identified. Whereas in the case of the $H^\bullet$ elimination step from $HOSO_2^-$ shown in Fig. 2, a lower barrier of 9.8 kcal/mol for the formation of *cis*-HONO and a higher barrier of 29.9 kcal/mol for *trans*-HONO have been

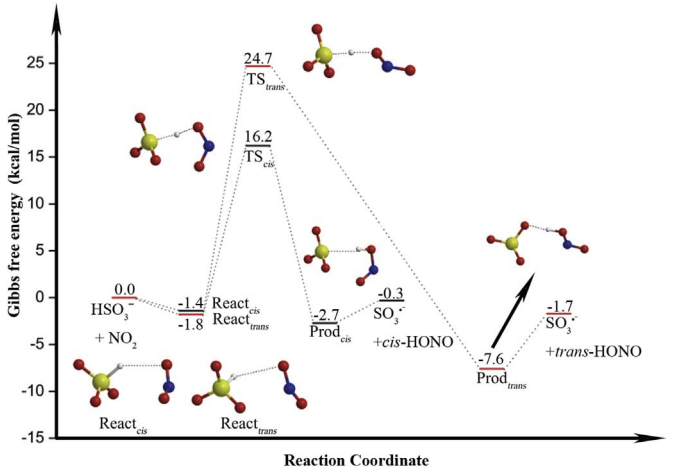

Fig. 1. Reaction energy profiles (kcal/mol) of the elimination of H• from HSO_3^- at CCSD (T)-F12/VDZ-F12//M06-2X/6-311 + + G(3df,3pd) level of theory. The white, blue, red and yellow spheres represent H, N, O and S atoms, respectively. (For interpretation of the references to colour in this figure legend, the reader is referred to the Web version of this article.)

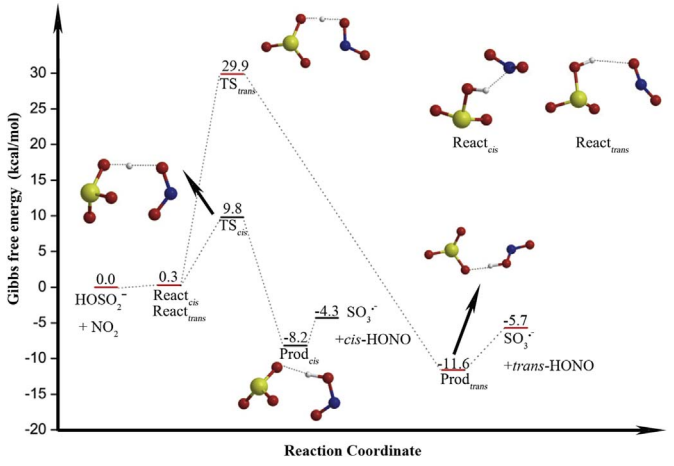

Fig. 2. Reaction energy profiles (kcal/mol) of the elimination of H• from $HOSO_2^-$ at CCSD(T)-F12/VDZ-F12//M06-2X/6-311 + + G(3df,3pd) level of theory. The white, blue, red and yellow spheres represent H, N, O and S atoms, respectively. (For interpretation of the references to colour in this figure legend, the reader is referred to the Web version of this article.)

identified. It is clear that the H• elimination step from $HOSO_2^-$ has the lowest reaction barrier of 9.5 kcal/mol relative to $React_{cis}$ with the formation of *cis*-HONO. The generated HONO can dissolve into the droplet to further dissociate to H^+ and NO_2^- or undergo reversible partitioning in the gas phase (Cheng et al., 2016). Moreover, HONO has been illustrated to represent an important gas-phase pollutant and can lead to a considerable production of hydroxyl radical (OH•) which in turn controls the oxidative capacity of atmosphere (Wang et al., 2015; Gligorovski, 2016; Xu et al., 2015; Kleffmann and Gavriloaiei, 2005; Su et al., 2008).

Meanwhile, in alkaline aerosol (pH > 7), the first step of the oxidation of SO_3^{2-} by NO_2 is an electron transfer step from SO_3^{2-} to NO_2 molecule (Eq. (4)) as suggested by Clifton (Clifton et al., 1988), leading the formation of $SO_3^{\bullet-}$ and NO_2^- with a gibbs free energy of 20.7 kcal/mol lower than that of SO_3^{2-} and NO_2. It is suggested by Clifton (Clifton et al., 1988; Spindler et al., 2003) that the initial step of the oxidation of aqueous SO_2 by NO_2 involves the formation of an addition complex $[NO_2\text{-}HSO_3]^-$ or $[NO_2\text{-}SO_3]^{2-}$ which will decompose to NO_2^- and $SO_3^{\bullet-}$. In this case, the calculations of corresponding complex show that the complex are not stable enough and will decompose directly to the products they proposed, which are exactly the products from H• elimination step (H^+, NO_2^- and $SO_3^{\bullet-}$) and electron transfer step (NO_2^- and $SO_3^{\bullet-}$) in the present study (Spindler et al., 2003).

3.1.2. The second and third steps in mechanism I for the subsequently oxidation of $SO_3^{\bullet-}$ by NO_2 in the aqueous water

The generated $SO_3^{\bullet-}$ in H• elimination step is an extremely active free radical and **S** atom presents an oxidation state of +5. In the droplet where a large amount of NO_2 radicals co-exist with $SO_3^{\bullet-}$, NO_2 can interact with $SO_3^{\bullet-}$ through the O-addition step expressed as Eq. (5) and Fig. 3(a) which is a barrier-less process, leading to the formation of SO_4NO^-. As the generated SO_4NO^- in the liquid environment is surrounded with water molecules, $React_{cis}$ and $React_{trans}$ shown in Fig. 3(b) have been identified to co-exist as reactants of the decomposition step of H_2O and hence lead to two parallel channels for the formation of $Prod_{cis}$ and $Prod_{trans}$, respectively. The decomposition step of H_2O (Eq. (7)) is a ring-opening reaction where the separated NO• from SO_4NO^- interacts with a OH• free radical separated from H_2O molecule to form a HONO molecule. Meanwhile, the left $SO_4^{\bullet-}$ and H• interact with each other, leading to the formation of HSO_4^- which will finally be dissociated in the aqueous water to H^+ and SO_4^{2-} ions. The energy barrier corresponding to TS_{cis} and TS_{trans} are 6.9 and 7.0 kcal/mol, respectively. Obviously, the two parallel channels have a similar energy barrier, making it possible for them to take place simultaneously.

3.1.3. The second and third steps in mechanism II for the subsequently oxidation of $SO_3^{\bullet-}$ by NO_2 in the aqueous water

An electron transfer step between $SO_3^{\bullet-}$ and NO_2 can also take place

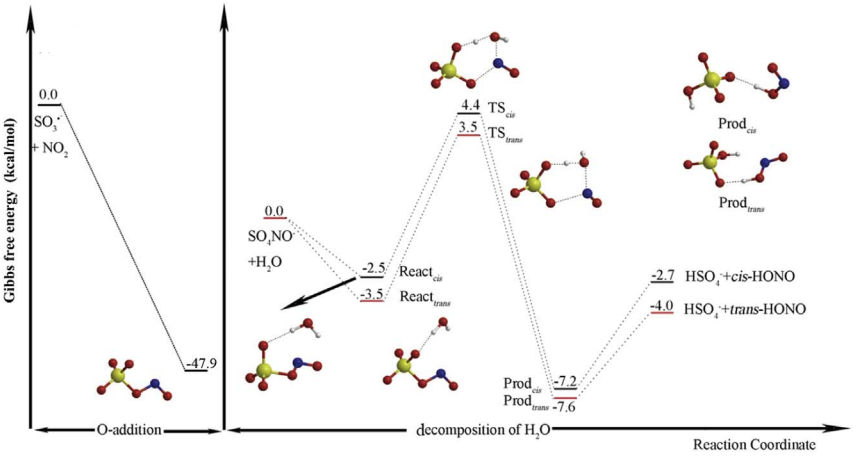

Fig. 3. Reaction energy profiles (kcal/mol) of (a) O-addition step and (b) decomposition of H_2O step at CCSD(T)-F12/VDZ-F12//M06-2X/6-311 + + G(3df,3pd) level of theory. The white, blue, red and yellow spheres represent H, N, O and S atoms, respectively. (For interpretation of the references to colour in this figure legend, the reader is referred to the Web version of this article.)

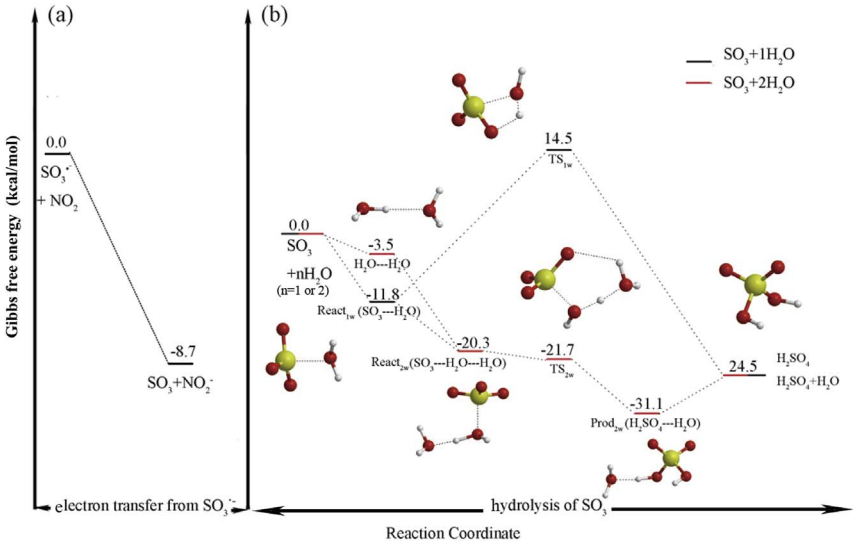

Fig. 4. Reaction energy profiles (kcal/mol) of (a) electron transfer step and (b) hydrolysis of SO_3 step at CCSD(T)-F12/VDZ-F12//M06-2X/6-311 + + G(3df,3pd) level of theory. The white, blue, red and yellow spheres represent H, N, O and S atoms, respectively. (For interpretation of the references to colour in this figure legend, the reader is referred to the Web version of this article.)

as expressed as Eq. (6) and shown in Fig. 4(a). The product SO_3 and NO_2^- are 8.7 kcal/mol lower than the reactants before electron transfer. The generated SO_3 molecule can undergo a hydrolysis process (Eq. (8)) with a barrier of 26.3 kcal/mol (TS_{1w} relative to $React_{1w}$), making contributions to the formation of $Prod_{1w}$ (H_2SO_4). It is worth noticing that, the hydrolysis of SO_3 has been extensively investigated both experimentally and theoretically over the past few years. In the gas phase, the reaction barrier can be significantly decreased by the participation of various species including water, water dimer (Morokuma and Muguruma, 1994), hydroperoxy radical (Gonzalez et al., 2010), formic acid (Hazra and Sinha, 2011), sulfuric acid (as autocatalyst) (Torrent-Sucarrat et al., 2012), nitric acid (Long et al., 2013) and ammonia molecules (Bandyopadhyay et al., 2017), acting as catalysts. In the liquid phase, there is also a facile SO_3 hydrolysis mechanism involving two explicit catalytic water molecules (Akhmatskaya et al., 1997; Larson et al., 2000). Hence, similar calculations for the catalytic effect of two water molecules ($React_{2w}$, TS_{2w} and $Prod_{2w}$) have been reproduced and shown in Fig. 4(b) in order to ensuer comparisons at a uniform level of theory. Apparently, the addition of the second water molecule make the hydrolysis step of SO_3 to be a barrierless process.

3.2. Kinetics and potential atmospheric impact

Overall, for the oxidation of HSO_3^- and $HOSO_2^-$ by NO_2 in the aqueous water, the first step - H• elimination step is the rate-limiting step. In order to confirm the main reaction pathway in the H• elimination step for HSO_3^- and $HOSO_2^-$, it is necessary to compare reaction rates rather than reaction rate constants expressed as Eq. (9). Therefore, the concentrations of reactants are taken into account, in addition to the reaction rate constant. Meanwhile, the tunneling effects could be quite profound for the H• elimination reactions which have a high imaginary frequency. Hence, the effect of tunneling on the H• elimination step is considered to enhance the specific reaction rate constant k_2 through the Wigner tunneling correction by a factor $\Gamma(T)$ (Wigner and Phys, 1932; Elm et al., 2013). By applying the steady-state conditions and assuming that the pre-reactive complex is in equilibrium with the reactant monomers, the overall rate constant k_{total} of the H• elimination step is obtained as Eq. (9) (Long et al., 2012; Fliegl et al., 2006; Zhu et al., 2017)

$$k_{total} = \frac{k_1}{k_{-1}}(\Gamma * k_2) = K_{eq} * (\Gamma * k_2) \tag{9}$$

where K_{eq} is the equilibrium constant expressed as Eq. (10) of the process $HSO_3^-/HOSO_2^- + NO_2 \rightarrow [HSO_3^- - NO_2]$ or $[HOSO_2^- - NO_2]$ complex of the H• elimination step, $\Gamma(T)$ is the tunneling effect factor for the H• elimination reactions expressed as Eq. (11) and k_2 is the reaction rate constant of the H• elimination step expressed as Eq. (12).

The equilibrium constant K_{eq} is calculated as Eq. (10)

$$K_{eq} = \exp\left(-\frac{\Delta G_{eq}}{RT}\right) \tag{10}$$

where ΔG_{eq} is the difference of the Gibbs free energy between the reactants complexes and the monomers, and R is the gas constant.

The tunneling effect factor $\Gamma(T)$ is given by Eq. (11) according to Wigner (Wigner and Phys, 1932; Elm et al., 2013)

$$\Gamma(T) = 1 + \frac{1}{24}\left(\frac{h\nu^{\mp}}{k_B T}\right)^2 \tag{11}$$

where h is the Planck constant, k_B is the Boltzmann constant, T is the temperature and $\nu^{\mp}$ is the frequency of the imaginary of the transition state.

The calculations of reaction rate constant of the H• elimination step from the pre-reactive complex utilizes the Transition State Theory (TST) expressed as Eq. (12) (Xie et al., 2010).

$$k_2 = (c^0)^{\Delta n}\frac{k_B T}{h}\exp\left(-\frac{\Delta G^0}{RT}\right) \tag{12}$$

where c^0 is the standard-state concentration (1 mol L^{-1}), Δn is the change of the number of moles from reactions to the transition states, h is the Planck constant, ΔG^0 (activation free energies) is the difference of the Gibbs free energy between the transition states and the reactants complexes, and R is the gas constant.

Overall, the reaction rates can be written as

$$\nu_{HSO_3^-} = k_{total-HSO_3^-}[NO_2][HSO_3^-] \tag{13}$$

$$\nu_{HOSO_2^-} = k_{total-HOSO_2^-}[NO_2][HOSO_2^-] \tag{14}$$

$$\frac{\nu_{HOSO_2^-}}{\nu_{HSO_3^-}} = \frac{k_{total-HOSO_2^-}[NO_2][HOSO_2^-]}{k_{total-HSO_3^-}[NO_2][HSO_3^-]} = \frac{k_{total-HOSO_2^-}[HOSO_2^-]}{k_{total-HSO_3^-}[HSO_3^-]} \tag{15}$$

Thus, the importance of H• elimination step of HSO_3^- and $HOSO_2^-$ depends not only on the rate constants but also on the relative concentrations of HSO_3^- and $HOSO_2^-$. As can be seen clearly from Figs. 1 and 2, the more favorable channel for the H• elimination of HSO_3^- or $HOSO_2^-$ is the one leading to the formation of *cis*-HONO, with barriers of 17.6 and 9.5 kcal/mol, respectively and the rate constant k_{total} of 30.98 and $2.67*10^6$ M^{-1} S^{-1} at 298.15 K, respectively.

As to the concentrations of HSO_3^- and $HOSO_2^-$, various experimental and theoretical studies dispute the relative stability of the HSO_3^- and $HOSO_2^-$ ions in the aqueous phase (Kahan et al., 2010; Hoffmann, 1986; Steudel and Steudel, 2009). Nevertheless, there is still not a consistent conclusion. A majority of the studies suggest that sulfonate HSO_3^- is the dominant species in the solution, while some experimental and theoretical studies suggest bisulfite $HOSO_2^-$ is in fact the dominant species (Kahan et al., 2010; Hoffmann, 1986; Steudel and Steudel, 2009; Ermakov et al., 1997; Horner and Connick, 1986; Risberg et al., 2007). In the present study, the reaction free energy for the interconvertion of HSO_3^- to $HOSO_2^-$ was determined to be 4.0 kcal/mol which was used to calculate the distribution of these two conformers at the equilibrium using the equation Eq. (16),

$$\frac{N_{HOSO_2^-}}{N_{HSO_3^-}} = e^{-\Delta G_{convert}/RT} \quad (16)$$

where $N_{HOSO_2^-}$ and $N_{HSO_3^-}$ are the amount of $HOSO_2^-$ and HSO_3^- conformers, respectively. And $\Delta G_{convert}$ is the reaction free energy from HSO_3^- to $HOSO_2^-$ interconvertion.

The proportion of $HOSO_2^-$ with HSO_3^- in the equilibrium was 1:858 which is in good agreement to the 1:200 ratio identified by experimental kinetics (Hoffmann, 1986). In this case, the ratio of the reaction rate expressed as Eq. (15) is 10^2, indicating that though HSO_3^- is thermodynamically more stable than $HOSO_2^-$, the main contribution to the missing sulfate production comes from the oxidation of $HOSO_2^-$ by the dissolved NO_2 in water. The corresponding rate constant k_{total} of the rate-limiting step ($H^{\bullet}$ elimination step) of $HOSO_2^-$ oxidized by NO_2 is $2.67*10^6\ M^{-1}\ S^{-1}$ at 298.15 K. While for the oxidation of SO_3^{2-}, the first and the second steps are both electron transfer processes and, hence, the third step becomes the rate-limiting step. As can be seen clearly from Figs. 3 and 4, although the hydrolysis of SO_3 step becomes a barrierless process with the aid of H_2O molecule in the aqueous water, the low energy barrier of 6.9 or 7.0 kcal/mol of the decomposition step of H_2O make it possible to be a parallel process with hydrolysis of SO_3 step. Another mechanism has also been proposed (Shen and Rochelle, 1998) and calculated, which has been identified uncompetitive with the mechanisms expressed in Eqs. (3) - (8) and shown as Eq. (17) - Eq. (18) in the Supplementary Information.

3.3. The tautomerization from HSO_3^- to $HOSO_2^-$

In the case that sulfonate HSO_3^- is the dominant species in the solution and is thermodynamically more stable than $HOSO_2^-$, however, the main contribution to the missing sulfate production comes from the oxidation of $HOSO_2^-$ and SO_3^{2-} by the dissolved NO_2 in water. For the aim of identifying the way HSO_3^- contributes to the formation of sulfate, the tautomerization from HSO_3^- to $HOSO_2^-$ is further studied in this section. As shown in Fig. 5, the tautomerization from HSO_3^- to $HOSO_2^-$ has a barrier of 53.8 kcal/mol (TS_{0w} relative to $React_{0w}$) without any catalysis. However, the addition of one (TS_{1w}) or two water molecules (TS_{2w}) as catalysts reveals a lower barrier of 38.7 and 31.8 kcal/mol. Even so, the reaction barrier is still too high for the direct tautomerization from HSO_3^- to $HOSO_2^-$. This is in consistence with Kahan's calculation results (Kahan et al., 2010). In this case, *cis*-HONO, HSO_4^- and sulfuric acid generated in the process may also participate in the tautomerization from HSO_3^- to $HOSO_2^-$ as catalysts. Remarkably shown in Fig. 6, the energy barrier is lowered to 17.1 kcal/mol through *cis*-HONO catalysis ($TS_{cis-HONO}$). Additionally, it is further reduced to 15.1, 12.3 and 11.6 kcal/mol with the aid of HSO_4^- ($TS_{HSO_4^-}$), *cis*-H_2SO_4 (TS_{cisSA}) and *trans*-H_2SO_4 ($TS_{transSA}$), respectively. Except the products $Prod_{cisSA}$ and $Prod_{transSA}$ with *cis*-H_2SO_4 and *trans*-H_2SO_4 molecule as catalysts, respectively, global products (global-*cis* and global-*trans*) have also been identified by manual research where a proton transfer occurred between the generated $HOSO_2^-$ and catalyst H_2SO_4 molecule, leading to the formation of H_2SO_3 and HSO_4^-. In this case, the H_2SO_3 will further be dissociated in the aqueous water to H^+, SO_3^{2-} and $HOSO_2^-$ ions which can be further oxidized by NO_2 in the aqueous water on one hand. On the other hand, the generated HSO_4^- can further catalyze the tautomerization from HSO_3^- to $HOSO_2^-$. It should be noticed that the generated H_2SO_4 molecule will finally be dissociated in the aqueous water to H^+ and SO_4^{2-} ions, hence it is not likely the main catalyst for the tautomerization from HSO_3^- to $HOSO_2^-$ in the aqueous water and the role of sulfuric acid as a catalyst

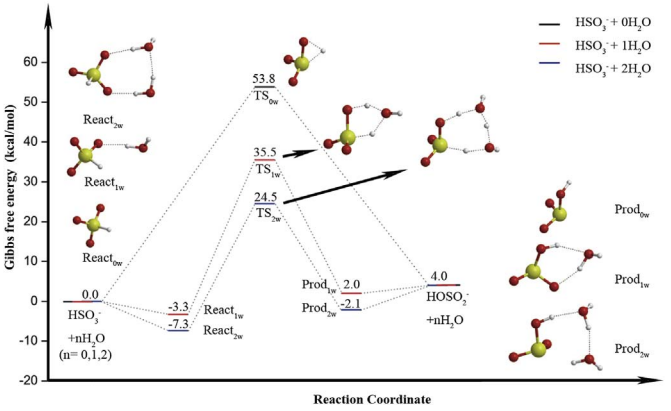

Fig. 5. Reaction energy profiles (kcal/mol) of the tautomerization from HSO_3^- to $HOSO_2^-$ with nH_2O molecules (n = 0, 1, 2) as the catalysts at CCSD(T)-F12/VDZ-F12//M06-2X/6-311 + + G(3df,3pd) level of theory. The white, blue, red and yellow spheres represent H, N, O and S atoms, respectively. (For interpretation of the references to colour in this figure legend, the reader is referred to the Web version of this article.)

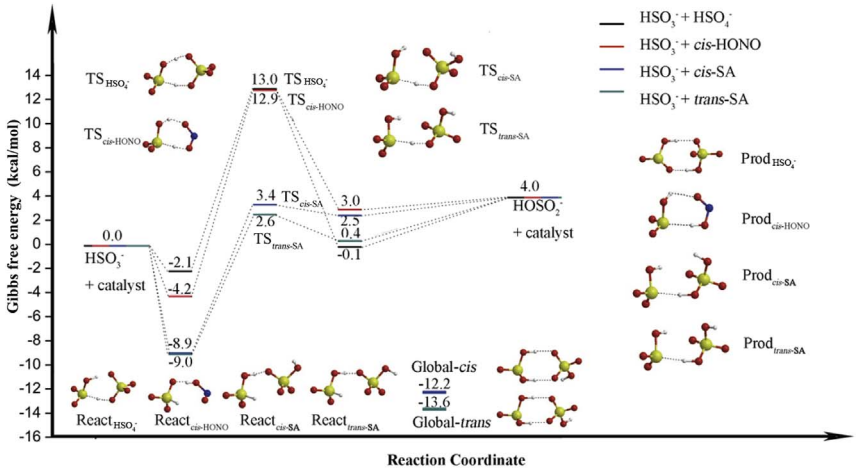

Fig. 6. Reaction energy profiles (kcal/mol) of the tautomerization from HSO_3^- to $HOSO_2^-$ with *cis*-HONO, HSO_4^- and H_2SO_4 (*trans*- and *cis*-) as the catalysts at CCSD(T)-F12/VDZ-F12//M06-2X/6-311 + + G(3df,3pd) level of theory. The white, blue, red and yellow spheres represent H, N, O and S atoms, respectively. (For interpretation of the references to colour in this figure legend, the reader is referred to the Web version of this article.)

should therefore be much more likely in the gas-phase. In this case, the whole process is a self-sustaining and continuous process.

4. Conclusion

Reactive nitrogen chemistry in aqueous water contributes significantly to the missing source of sulfate during the haze period in China. Two feasible mechanisms have been proposed and calculated for the oxidation of SO_2 by the dissolved NO_2 in the aqueous water. In weakly acidic and neutral aerosol (pH ≤ 7), the main contribution to the missing sulfate production comes from the oxidation of $HOSO_2^-$ by the dissolved NO_2 in water,and the whole process is a self-sustaining process where the generated *cis*-HONO, HSO_4^- and H_2SO_4 could further promote the tautomerization from HSO_3^- to $HOSO_2^-$ as catalysts efficiently and the catalytic efficiency is in the order of *trans*-H_2SO_4 > *cis*-H_2SO_4 > HSO_4^- > *cis*-HONO > $(H_2O)_2$ > H_2O. In the alkaline aerosol (pH > 7), the main contribution to the missing sulfate production comes from the oxidation of SO_3^{2-} where the third step - decomposition step of H_2O or hydrolysis of SO_3 step which are two parallel processes are the rate-limiting step. The present results are of avail to better understand the missing source of sulfate in the aerosol and hence may lead to better science-based solutions for resolving the severe haze problems in China. Potentially other radical reactions such as with $OH^{\bullet}$ or criegee intermediates could also be the source of sulfate and need to be further studied.

Acknowledgements

The authors are indebted to the Chinese National Natural Science Foundation (Grant Nos. 21373025, 91544223, 21473010, 21673018 and 21673019) for the support of this research.

Appendix A. Supplementary data

Supplementary data related to this article can be found at http://dx.doi.org/10.1016/j.atmosenv.2018.01.017.

References

Ajdari, S., Normann, F., Andersson, K., Johnsson, F., 2016. Reduced mechanism for nitrogen and sulfur chemistry in pressurized flue gas systems. Ind. Eng. Chem. Res. 55 (19), 5514–5525.

Akhmatskaya, E.V., Apps, C.J., Hillier, I.H., Masters, A.J., Palmer, I.J., Watt, N.E., Vincent, M.A., Whitehead, J.C., 1997. Hydrolysis of SO_3 and $ClONO_2$ in water clusters a combined experimental and theoretical study. J. Chem. Soc. Faraday. Trans. 93 (16), 2775–2779. http://dx.doi.org/10.1039/a701768e.

Bandyopadhyay, B., Kumar, P., Biswas, P., 2017. Ammonia catalyzed formation of sulfuric acid in troposphere: the curious case of a base promoting acid rain. J. Phys. Chem. 121 (16), 3101–3108. http://dx.doi.org/10.1021/acs.jpca.7b01172.

Brown, R.E., Barber, F., 1995. Ab initio studies of the thermochemistry of the bisulfite and the sulfonate ions and related compounds. J. Phys. Chem. 99 (20), 8071–8075. http://dx.doi.org/10.1021/j100020a034.

Cheng, Y., Zheng, G., Wei, C., Mu, Q., Zheng, B., Wang, Z., Gao, M., Zhang, Q., He, K., Carmichael, G., Pöschl, U., Su, H., 2016. Reactive nitrogen chemistry in aerosol water as a source of sulfate during haze events in China. Science Advances 2. http://dx.doi.org/10.1126/sciadv.1601530.

Clifton, C.L., Altstein, N., Hule, R.E., 1988. Rate constant for the reaction of NO_2 with sulfur(IV) over the pH range 5.3-13. Environ. Sci. Technol. 22 (5), 586–589. http://dx.doi.org/10.1021/es00170a018.

Cossi, M., Rega, N., Scalmani, G., Barone, V., 2003. Energies, structures, and electronic properties of molecules in solution with the C-PCM solvation model. J. Comput. Chem. 24 (6), 669–681. http://dx.doi.org/10.1002/jcc.10189.

Delabie, A., Creve, S., Coussens, B., Nguyen, M.T., 2000. Theoretical study of the solvent effect on the hydrogen abstraction reaction of the methyl radical with hydrogen peroxide. J. Chem. Soc. Perkin Trans. 2 (5), 977–981. http://dx.doi.org/10.1039/b000143k.

Dong, K., Sun, C.H., Zhang, S., Wang, H.Y., Song, J.W., Pang, S.P., 2017. Condensation mechanism of cage hexabenzylhexaazaisowurtzitane from glyoxal and benzylamine: a computational study. N. J. Chem. 41, 12694–12699. http://dx.doi.org/10.1039/c7nj00972k.

Elm, J., Bilde, M., Mikkelsen, K.V., 2012. Assessment of density functional theory in predicting structures and free energies of reaction of atmospheric prenucleation clusters. J. Chem. Theor. Comput. 8 (6), 2071–2077. http://dx.doi.org/10.1021/ct300192p.

Elm, J., Jørgensen, S., Bilde, M., Mikkelsen, K.V., 2013. Ambient reaction kinetics of atmospheric oxygenated organics with the OH radical: a computational methodology study. Phys. Chem. Chem. Phys. 15 (24), 9636–9645. http://dx.doi.org/10.1039/c3cp50192b.

Elm, J., Passananti, M., Kurtén, T., Vehkamäki, H., 2017. Diamines can initiate new particle formation in the atmosphere. J. Phys. Chem. 121 (32), 6155–6164. http://dx.doi.org/10.1021/acs.jpca.7b05658.

Ermakov, A.N., Poskrebyshev, G.A., Purmal, A.P., 1997. Sulfite oxidation: the state-of-the-art of the problem. Kinet. Catal. 38 (3), 295–308.

Fliegl, H., Glöβ, A., Welz, O., Olzmann, M., Klopper, W., 2006. Accurate computational determination of the binding energy of the SO3•H2O complex. J. Chem. Phys. 125 (5), 054312. http://dx.doi.org/10.1063/1.2234372.

Frisch, M.J., Trucks, G.W., Schlegel, H.B., Scuseria, G.E., Robb, M.A., Cheeseman, J.R., Scalmani, G., Barone, V., Mennucci, B., Petersson, G.A., Nakatsuji, H., Caricato, M., Li, X., Hratchian, H.P., Izmaylov, A.F., Bloino, J., Zheng, G., Sonnenberg, J.L., Hada, M., Ehara, M., Toyota, K., Fukuda, R., Hasegawa, J., Ishida, M., Nakajima, T., Honda, Y., Kitao, O., Nakai, H., Vreven, T., Montgomery, J.A., Peralta, J.E., Ogliaro, F., Bearpark, M., Heyd, J.J., Brothers, E., Kudin, K.N., Staroverov, V.N., Kobayashi, R., Normand, J., Raghavachari, K., Rendell, A., Burant, J.C., Iyengar, S.S., Tomasi, J., Cossi, M., Rega, N., Millam, J.M., Klene, M., Knox, J.E., Cross, J.B., Bakken, V., Adamo, C., Jaramillo, J., Gomperts, R., Stratmann, R.E., Yazyev, O., Austin, A.J., Cammi, R., Pomelli, C., Ochterski, J.W., Martin, R.L., Morokuma, K., Zakrzewski, V.G., Voth, G.A., Salvador, P., Dannenberg, J.J., Dapprich, S., Daniels, A.D., Farkas, O., Foresman, J.B., Ortiz, J.V., Cioslowski, J., Fox, D.J., 2009. Gaussian 09, Revision A.01. Gaussian Inc., Wallingford CT.

Gao, M., Carmichael, G. R., Wang, Y., Ji, D., Liu, Z., Wang, Z., Improving simulations of sulfate aerosols during winter haze over northern China: the impacts of heterogeneous oxidation by NO_2, Front. Environ. Sci. Eng. 10(5). https://doi.org/10.1007/s11783-016-0878-2.

Gligorovski, S., 2016. Nitrous acid (HONO): an emerging indoor pollutant. J. Photochem. Photobiol. Chem. 314, 1–5. http://dx.doi.org/10.1016/j.jphotochem.2015.06.008.

Gonzalez, C., Schlegel, H.B., 1989. An improved algorithm for reaction path following. J. Chem. Phys. 90 (4), 2154–2161. http://dx.doi.org/10.1063/1.456010.

Gonzalez, J., Torrent-Sucarrat, M., Anglada, J.M., 2010. The reactions of SO_3 with HO_2 radical and H_2O …HO_2 radical complex. theoretical study on the atmospheric formation of HSO_5 and H_2SO_4. Phys. Chem. Chem. Phys. 12 (9), 2116–2125. http://dx.doi.org/10.1039/b916659a.

Hazra, M.K., Sinha, A., 2011. Formic acid catalyzed hydrolysis of SO_3 in the gas phase: a barrierless mechanism for sulfuric acid production of potential atmospheric importance. J. Am. Chem. Soc. 133 (43), 17444–17453. http://dx.doi.org/10.1021/ja207393v.

Hoffmann, M.R., 1986. On the kinetics and mechanism of oxidation of aquated sulfur-dioxide by ozone. Atmos. Environ. 20 (6), 1145–1154. http://dx.doi.org/10.1016/0004-6981(86)90147-2.

Horner, D.A., Connick, R.E., 1986. Equilibrium quotient for the isomerization of bisulfite from HSO_3 to SO_3H^-. Inorg. Chem. 25 (14), 2414–2417. http://dx.doi.org/10.1021/ic00234a026.

Hoyle, C.R., Fuchs, C., Järvinen, E., Saathoff, H., Dias, A., El Haddad, I., Gysel, M., Coburn, S.C., Tröstl, J., Bernhammer, A.K., Bianchi, F., Breitenlechner, M., Corbin, J.C., Craven, J., Donahue, N.M., Duplissy, J., Ehrhart, S., Frege, C., Gordon, H., Höppel, N., Heinritzi, M., Kristensen, T.B., Molteni, U., Nichman, L., Pinterich, T., Prévôt, A.S.H., Simon, M., Slowik, J., Steiner, G., Tomé, A., Vogel, A.L., Volkamer, R., Wagner, A.C., Wangner, R., Wexler, A.S., Williamson, C., Winkler, P.M., Yan, C., Amorim, A., Dommen, J., Curtius, J., Gallagher, M.W., Flagan, R.C., Hansel, A., Kirkby, J., Kulmala, M., Möhler, O., Stratmann, F., Worsnop, D.R., Baltensperger, U., 2016. Aqueous phase oxidation of sulphur dioxide by ozone in cloud droplets. Atmos. Chem. Phys. 16 (3), 1693–1712. http://dx.doi.org/10.5194/acp-16-1693-2016.

Huang, X., Song, Y., Zhao, C., Li, M., Zhu, T., Zhang, Q., Zhang, X., 2014. Pathways of sulfate enhancement by natural and anthropogenic mineral aerosols in China. J. Geophys. Res. Atmos. 119 (24), 735–753. http://dx.doi.org/10.1002/2014JD022301.

Kahan, T.F., Ardura, D., Donaldson, D.J., 2010. Mechanism of aqueous-phase ozonation of S(IV). J. Phys. Chem. B 114 (5), 2164–2170. http://dx.doi.org/10.1021/jp9085156.

Kleffmann, J., Gavriloaiei, T., 2005. Daytime formation of nitrous acid: a major source of oh radicals in a forest. Geophys. Res. Lett. 32, L05818. http://dx.doi.org/10.1029/2005GL022524.

Knizia, G., Adler, T.B., Werner, H.J., 2009. Simplified CCSD(T)-F12 methods: theory and benchmarks. J. Chem. Phys. 130 (5), 054104. http://dx.doi.org/10.1063/1.3054300.

Lane, J.R., Kjaergaard, H.G., 2009. Explicitly correlated intermolecular distances and interaction energies of hydrogen bonded complexes. J. Chem. Phys. 131 (3), 034307. http://dx.doi.org/10.1063/1.3159672.

Larson, L.J., Kuno, M., Tao, F.M., 2000. Hydrolysis of sulfur trioxide to form sulfuric acid in small water clusters. J. Chem. Phys. 112 (20), 8830–8838. http://dx.doi.org/10.1063/1.481532.

Laskin, A., Gaspar, D.J., Wang, W., Hunt, S.W., Cowin, J.P., Colson, S.D., Finlayson-Pitts, B.J., 2003. Reactions at interfaces as a source of sulfate formation in sea-salt particles. Science 301 (5631), 340–344. http://dx.doi.org/10.1126/science.1085374.

Lee, Y.N., Schwartz, S.E., 1982. Kinetics of Oxidation of Aqueous Sulfur(IV) by Nitrogen Dioxide.

Li, G., Zhang, R., Fan, J., Tie, X., 2005. Impacts of black carbon aerosol on photolysis and ozone. J. Geophys. Res. Atmos. 110 (D23), D23206. http://dx.doi.org/10.1029/2005JD005898.

Li, L., Kumar, M., Zhu, C., Zhong, J., Francisco, J.S., Zeng, X.C., 2016. Near-barrierless ammonium bisulfate formation via a loop-structure promoted proton-transfer mechanism on the surface of water. J. Am. Chem. Soc. 138 (6), 1816–1819. http://dx.

doi.org/10.1021/jacs.5b13048.
Li, S., Du, L., Wei, Z., Wang, W., 2017. Aqueous-phase aerosols on the air-water interface: response of fatty acid Langmuir monolayers to atmospheric inorganic ions. Sci. Total Environ. 580, 1155–1161. http://dx.doi.org/10.1016/j.scitotenv.2016.12.072.
Liu, S., Jia, L., Xu, Y., Tsona, N.T., Ge, S., Du, L., 2017. Photooxidation of cyclohexene in the presence of SO_2: SOA yield and chemical composition. Atmos. Chem. Phys. 17 (21), 13329–13343. http://dx.doi.org/10.5194/acp-17-13329-2017.
Long, B., Long, Z.W., Wang, Y.B., Tan, X.F., Han, Y.H., Long, C.Y., Qin, S.J., Zhang, W.J., 2012. Formic acid catalyzed gas-phase reaction of H2O with SO3 and the reverse reaction: a theoretical study. ChemPhysChem 13 (1), 323–329. http://dx.doi.org/10.1002/cphc.201100558.
Long, B., Chang, C.R., Long, Z.W., Wang, Y.B., Tan, X.F., Zhang, W.J., 2013. Nitric acid catalyzed hydrolysis of SO_3 in the formation of sulfuric acid: a theoretical study. Chem. Phys. Lett. 581, 26–29. http://dx.doi.org/10.1016/j.cplett.2013.07.012.
Mardirossian, N., Head-Gordon, M., 2016. How accurate are the Minnesota density functionals for noncovalent interactions, isomerization energies, thermochemistry, and barrier heights involving molecules composed of main-group elements? J. Chem. Theor. Comput. 12 (9), 4303–4325. http://dx.doi.org/10.1021/acs.jctc.6b00637.
Morokuma, K., Muguruma, C., 1994. Ab initio molecular orbital study of the mechanism of the gas phase reaction $SO_3 + H_2O$: importance of the second water molecule. J. Am. Chem. Soc. 116 (22), 10316–10317. http://dx.doi.org/10.1021/ja00101a068.
Myllys, N., Olenius, T., Kurtén, T., Vehkamäki, H., Riipinen, I., Elm, J., 2017. The effect of bisulfate, ammonia, and ammonium on the clustering of organic acids and sulfuric acid. J. Phys. Chem. 121 (25), 4812–4824. http://dx.doi.org/10.1021/acs.jpca.7b03981.
Neese, F., 2012. The orca program system. Wiley interdiscipl. Rev. Comput. Mol. Sci. 2, 73–78.
Pereira, A.T., Ribeiro, A.J.M., Fernandes, P.A., Ramos, M.J., 2017. Benchmarking of density functionals for the kinetics and thermodynamics of the hydrolysis of glycosidic bonds catalyzed by glycosidases. Int. J. Quant. Chem. 117 (18), e25409. http://dx.doi.org/10.1002/qua.25409.
Peterson, K.A., Adler, T.B., Werner, H.J., 2008. Systematically convergent basis sets for explicitly correlated wavefunctions: the atoms H, He, B - Ne, and Al - Ar. J. Chem. Phys. 128 (8), 084102. http://dx.doi.org/10.1063/1.2831537.
Risberg, E.D., Eriksson, L., Mink, J., Pettersson, L.G.M., Skripkin, M.Y., SandströM, M., 2007. Sulfur x-ray absorption and vibrational spectroscopic study of sulfur dioxide, sulfite, and sulfonate solutions and of the substituted sulfonate ions $X_3CSO_3^-$ (X = H, Cl, F). Inorg. Chem. 46 (20), 8332–8348. http://dx.doi.org/10.1021/ic062440i.
Rohrer, F., Berresheim, H., Strong correlation between levels of tropospheric hydroxyl radicals and solar ultraviolet radiation. Nature 442(7099), 184–187. https://doi.org/10.1038/nature04924.
Shen, C.H., Rochelle, G.T., 1998. Nitrogen dioxide absorption and sulfite oxidation in aqueous sulfite. Environ. Sci. Technol. 32 (13), 1994–2003. http://dx.doi.org/10.1021/es970466q.
Shi, G., Xu, J., Peng, X., Xiao, Z., Chen, K., Tian, Y., Guan, X., Feng, Y., Yu, H., Nenes, A., Russel, A.G., 2017. pH of aerosols in a polluted atmosphere: source contributions to highly acidic aerosol. Environ. Sci. Technol. 51 (8), 4289–4296. http://dx.doi.org/10.1021/acs.est.6b05736.
Spindler, G., Hesper, J., Brüggemann, E., Dubois, R., Müller, T., Herrmann, H., 2003. Wet annular denuder measurements of nitrous acid: laboratory study of the artefact reaction of NO2 with S(IV) in aqueous solution and comparison with field measurements. Atmos. Environ. 37 (19), 2643–2662. http://dx.doi.org/10.1016/S1352-2310(03)00209-7.
Steudel, R., Steudel, Y., 2009. Sulfur dioxide and water: structures and energies of the hydrated species $SO_2 \cdot nH_2O$, $[HSO_3]^- \cdot nH_2O$, $[SO_3H]^- \cdot nH_2O$ and $H_2SO_3 \cdot nH_2O$ (n = 0-8). Eur. J. Inorg. Chem. 10, 1393–1405. http://dx.doi.org/10.1002/ejic.200801158.
Su, H., Cheng, Y.F., Shao, M., Gao, D.F., Yu, Z.Y., Zeng, L.M., Slanina, J., Zhang, Y.H., Wiedensohler, A., 2008. Nitrous acid (HONO) and its daytime sources at a rural site during the 2004 prideprd experiment in China. J. Geophys. Res. Atmos. 113 (D14), D14312. http://dx.doi.org/10.1029/2007JD009060.
Sun, X., Zhang, C., Zhao, Y., Bai, J., Zhang, Q., Wang, W., 2012. Atmospheric chemical reactions of 2,3,7,8-tetrachlorinated dibenzofuran initiated by an OH radical: mechanism and kinetics study. Environ. Sci. Technol. 46 (15), 8148–8155. http://dx.doi.org/10.1021/es301413v.
Takano, Y., Houk, K.N., 2005. Benchmarking the conductor-like polarizable continuum model (CPCM) for aqueous solvation free energies of neutral and ionic organic molecules. J. Chem. Theor. Comput. 1 (1), 70–77. http://dx.doi.org/10.1021/ct049977a.
Tie, X., Madronich, S., Walters, S., Zhang, R., Rasch, P., Collins, W., 2003. Effect of clouds on photolysis and oxidants in the troposphere. J. Geophys. Res. Atmos. 108 (D20), 4642. http://dx.doi.org/10.1029/2003JD003659.
Torrent-Sucarrat, M., Francisco, J.S., Anglada, J.M., 2012. Sulfuric acid as autocatalyst in the formation of sulfuric acid. J. Am. Chem. Soc. 134 (51), 20632–20644. http://dx.doi.org/10.1021/ja307523b.
Vchirawongkwin, V., Pornpiganon, C., Kritayakornupong, C., Tongraar, A., Rode, B.M., 2012. The stability of bisulfite and sulfonate ions in aqueous solution characterized by hydration structure and dynamics. J. Phys. Chem. B 116 (37), 11498–11507. http://dx.doi.org/10.1021/jp305648e.
Wang, L., Wen, L., Xu, C., Chen, J., Wang, X., Yang, L., Wang, W., Yang, X., Sui, X., Yao, L., Zhang, Q., 2015. HONO and its potential source particulate nitrite at an urban site in north China during the cold season. Sci. Total Environ. 538, 93–101. http://dx.doi.org/10.1016/j.scitotenv.2015.08.032.
Wang, G., Zhang, R., Gomez, M.E., Yang, L., Zamora, M.L., Hu, M., Lin, Y., Peng, J., Guo, S., Meng, J., Li, J., Cheng, C., Hu, T., Ren, Y., Wang, Y., Gao, J., An, Z., Zhou, W., Li, G., Wang, J., Tian, P., Marrero-Ortiz, W., Secrest, J., Du, Z., Zheng, J., Shang, D., Zeng, L., Shao, M., Wang, W., Huang, Y., Wang, Y., Zhu, Y., Li, Y., Hu, J., Pan, B., Cai, L., Cheng, y. Ji, F. Zhnag, D. Rosenfeld, P. S. Liss, R. A. Duce, C. E. Kolb, M. J. Molina, Y., 2016. Persistent sulfate formation from london fog to Chinese haze. Proc. Natl. Acad. Sci. U.S.A. 113 (48), 13630–13635. http://dx.doi.org/10.1073/pnas.1616540113.
Wigner, E., Phys, Z., 1932. Chem. Abt. B 19, 203–216.
Xie, H.B., Zhou, Y., Zhang, Y., Johnson, J.K., 2010. Reaction mechanism of monoethanolamine with co in aqueous solution from molecular modeling. J. Phys. Chem. 114 (43), 11844–11852. http://dx.doi.org/10.1021/jp107516k.
Xu, F., Wang, H., Zhang, Q., Zhang, R., Qu, X., Wang, W., 2010. Kinetic properties for the complete series reactions of chlorophenols with oh radicals-relevance for dioxin formation. Environ. Sci. Technol. 44 (4), 1399–1404. http://dx.doi.org/10.1021/es9031776.
Xu, Z., Wang, T., Wu, J., Xue, L., Chan, J., Zha, Q., Zhou, S., Louie, P.K.K., Luk, C.W.Y., 2015. Nitrous acid (HONO) in a polluted subtropical atmosphere: seasonal variability, direct vehicle emissions and heterogeneous production at ground surface. Atmos. Environ. 106, 100–109. http://dx.doi.org/10.1016/j.atmosenv.2015.01.061.
Xue, J., Yuan, Z., Griffith, S.M., Yu, X., Lau, A.K.H., Yu, J.Z., 2016. Sulfate formation enhanced by a cocktail of high NO_x, SO_2, particulate matter, and droplet pH during haze-fog events in megacities in China: an observation-based modeling investigation. Environ. Sci. Technol. 50 (14), 7325–7334. http://dx.doi.org/10.1021/acs.est.6b00768.
Yousaf, K.E., Peterson, K.A., 2008. Optimized auxiliary basis sets for explicitly correlated methods. J. Chem. Phys. 129 (18), 184108. http://dx.doi.org/10.1063/1.3009271.
Zhang, Q., Gao, R., Xu, F., Zhou, Q., Jiang, G., Wang, T., Chen, J., Hu, J., Jiang, W., Wang, W., 2014. Role of water molecule in the gas-phase formation process of nitrated polycyclic aromatic hydrocarbons in the atmosphere: a computational study. Environ. Sci. Technol. 48 (9), 5051–5057. http://dx.doi.org/10.1021/es500453g.
Zhang, R., Wang, G., Guo, S., Zamora, M.L., Ying, Q., Lin, Y., Wang, W., Hu, M., Wang, Y., 2015. Formation of urban fine particulate matter. Chem. Rev. 115 (10), 3803–3855. http://dx.doi.org/10.1021/acs.chemrev.5b00067.
Zhao, Y., Truhlar, D.G., 2008. The M06 suite of density functionals for main group thermochemistry, thermochemical kinetics, noncovalent interactions, excited states, and transition elements: two new functionals and systematic testing of four M06-class functionals and 12 other functionals. Theor. Chem. Acc. 120 (1–3), 215–241. http://dx.doi.org/10.1007/s00214-007-0310-x.
Zheng, B., Zhang, Q., Zhang, Y., He, K.B., Wang, K., Zheng, G.J., Duan, F.K., Ma, Y.L., Kimoto, T., 2015. Heterogeneous chemistry: a mechanism missing in current models to explain secondary inorganic aerosol formation during the january 2013 haze episode in north China. Atmos. Chem. Phys. 14 (15), 2031–2049. http://dx.doi.org/10.5194/acp-15-2031-2015.
Zheng, G. J., Duan, F. K., Su, H., Ma, Y. L., Cheng, Y., Zheng, B., Zhang, Q., Huang, T., Kimoto, T., Chang, D., Pöschl, U., Cheng, Y. F., He, K. B., Exploring the severe winter haze in beijing: the impact of synoptic weather, regional transport and heterogeneous reactions, Atmos. Chem. Phys. 15(6), 2969–2983. https://doi.org/10.5194/acp-15-2969-2015.
Zhu, J., Wang, S., Tsona, N.T., Jiang, X., Wang, Y., Ge, M., Du, L., 2017. Gas phase reaction of methyl n-propyl ether with OH, NO_3 and Cl: kinetics and mechanism. J. Phys. Chem. 121 (36), 6800–6809. http://dx.doi.org/10.1021/acs.jpca.7b06877.